NOTE • OPEN ACCESS

A comparison of measured and treatment planning system out-of-field dose for a 1.5 T MR linac

IOP Publishing Phys. Med. Biol. 68 (2023) 20NT01 https://doi.org/10.1088/1361-6560/acf912

Physics in Medicine & Biology

IPEM Institute of Physics and Engineering in Medicine

NOTE

A comparison of measured and treatment planning system out-of-field dose for a 1.5 T MR linac

Marcus Powers[1,2,*] and **John Baines**[1,2]

[1] Townsville Cancer Centre, Townsville Hospital and Health Service, Townsville, Queensland, Australia
[2] College of Science and Engineering, James Cook University, Townsville, Queensland, Australia
[*] Author to whom any correspondence should be addressed.

E-mail: marcus.powers@my.jcu.edu.au

Keywords: out-of-field dose, electron streaming effect, spiralling contaminant electrons, elekta unity, monaco

OPEN ACCESS

RECEIVED
20 September 2022

REVISED
1 September 2023

ACCEPTED FOR PUBLICATION
12 September 2023

PUBLISHED
2 October 2023

Abstract

Objective. Dose due to the electron streaming effect (ESE) is a significant contribution to out-of-field dose on the Elekta Unity MR-Linac. The aim of this work is to provide a systematic comparison of calculated and measured streaming dose for this system. *Approach.* Beams 1.0×1.0 cm^2 to 5.0×5.0 cm^2, gantry 90.0°, 1000 MU, were incident on an in-house phantom. At the beam entrance and exit surfaces of the phantom, ESE was generated in the *Y*-direction (IEC 61217). EBT3 film, orientated within the *X*–*Z* plane and at 14.0 mm depth in a solid water block, was used to determine ESE dose 5.0 cm beyond the phantom. The experimental arrangement was simulated in the Monaco v5.4 treatment planning system (TPS), utilising a CT phantom dataset with differing relative electron densities (RED) for the surrounding air. Horizontal (*X* direction) and vertical (*Z* direction) film dose profiles were compared to the corresponding TPS profiles. *Main results.* For each field, the maximum ESE dose was observed at the beam exit, the magnitude of which decreases with decreasing field size. For the 5.0×5.0 cm^2 field, the exit and entry ESE doses were 19.6% and 7.0% of the D_{max} dose to water, respectively. Across horizontal profiles, differences (simulated—measured) were reduced with smaller fields and lower RED. The maximum absolute profile difference was 1.7% of the D_{max} dose to water for optimal RED and isocentre location. In vertical profiles an offset consistent with the Lorentz force was observed relative to the *X*–*Y* isoplane. *Significance.* For the fields investigated, maximum absolute differences (simulated—measured) $\leqslant$ 5.2% occurred in peak regions of ESE, at the beam entrance and exit from the phantom. Generally, there is good agreement between Monaco simulated and measured ESE. Simulated out-of-field dose is sensitive to the RED assigned to air structures and unforced RED optimises out-of-field dose calculation accuracy.

Introduction

The presence of a magnetic field around the patient in MR-Linacs (MRLs), such as the Elekta Unity (Stockholm, Sweden), gives rise to contributions to out-of-field dose (OFD) that are unique to these systems (Hackett *et al* 2018, Malkov *et al* 2019b, Baines *et al* 2021, Powers and Baines 2022). OFD on the Unity is a combination of these sources, namely spiralling contaminant electrons and electron streams, as well as the head leakage and scatter common to all linacs. As described in other works (Raaymakers *et al* 2009, Raaymakers *et al* 2017, Snyder *et al* 2020, Woodings *et al* 2021) the Unity integrates MR imaging and a 7 MV flattening filter free(FFF) x-ray source. The source is mounted on an annular gantry that is free to rotate around a cylindrical MR imaging system, a modified Philips Ingenia 1.5 T MRI. With this geometry the plane of rotation of the source is perpendicular to the static field (B_0). The relative orientation of B_0 ($-Y$ direction IEC61217) and the beam direction (within the *X*–*Z* plane IEC61217) will, via the Lorentz force, influence the trajectory of secondary electrons set in motion by the beam.

Consequently, within the Unity bore secondary electrons exiting a patient interact with B_0 giving rise to either the electron return effect (ERE) (Raaijmakers *et al* 2005), which increases skin dose (Nachbar *et al* 2020),

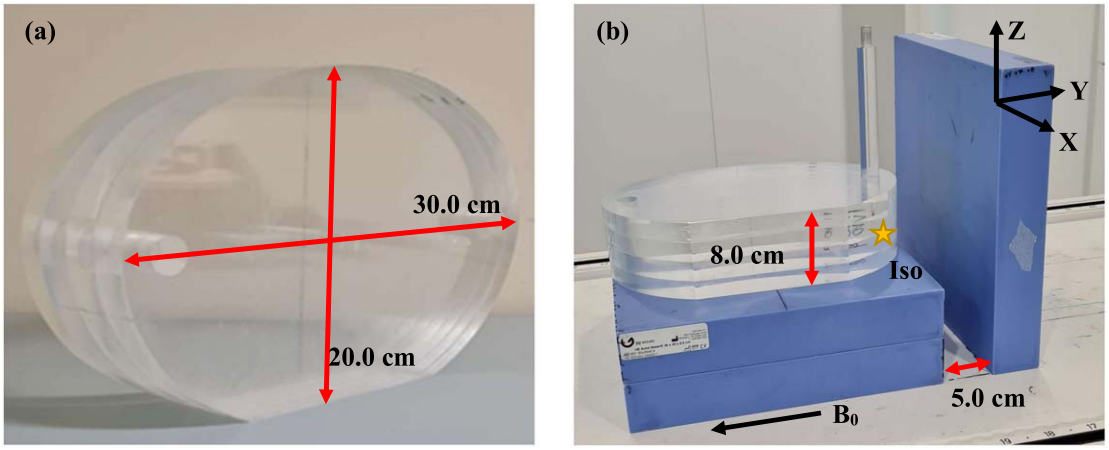

Figure 1. (a) The acrylic phantom used to investigate ESE. Holes in the phantom are plugged with rods to align the slabs and remove air cavities. In (b) the phantom in situ is displayed, with IEC61217 coordinate system.

or the electron streaming effect (ESE) which may cause OFD deposition to patient surfaces in the cranio-caudal ($\pm Y$) direction (Park *et al* 2018, Baines *et al* 2021, De-Colle *et al* 2021). For the latter, electrons interacting with B_0 follow spiral trajectories parallel and antiparallel to the static field. Similarly, air ionisation in the beam path produces so called spiralling contaminant electrons (SCE) which may also contribute to OFD in the $\pm Y$ directions (Hackett *et al* 2018, Malkov *et al* 2019a). A reported increase in skin V_{35Gy} during partial breast irradiation was 24.9%–40.2%, due to ERE in the presence of a 1.5 T field (Nachbar *et al* 2020). *In vivo* measurements of ESE dose indicated between 16.0%–30.0% of the prescription dose (Park *et al* 2018, Lui *et al* 2020, Baines *et al* 2021) was observed out-of-field, significantly larger than the OFD attributed to SCE (Baines *et al* 2021). In a phantom study of ESE, Monte Carlo simulations predicted a maximum ESE dose of 39.0% of D_{max} (Malkov *et al* 2019a).

The average energy of streaming electrons is approximately 500.0 keV (Raaijmakers *et al* 2005) and 1.0 cm of tissue-equivalent material is sufficient to shield patient surfaces in the path of such electrons (Park *et al* 2018). The Elekta Unity treatment planning system (TPS), Monaco v5.40, enables ESE to be visualised (Baines *et al* 2021, Powers and Baines 2022) and patient surfaces requiring shielding can be identified. It has been shown that *in vivo* measurements of ESE are in general agreement with TPS calculations (Nachbar *et al* 2020, Baines *et al* 2021). However, to date a systematic quantitative investigation comparing TPS ESE dose with measured data has not been reported. This study aims to address this and to the best of our knowledge the work presented is the first such evaluation of the Unity TPS to be reported.

Materials and methods

Experimental details

To generate electron streams, an in-house thorax phantom was adapted for use in this investigation. This phantom is a shoulder analogue, and it was previously reported that in a Unity treatment of an SCF lesion significant OFD due to electron streams was generated at beam entrance and exit locations (Baines *et al* 2021). The phantom consists of four acrylic slabs, 2.0 cm thick, 30.0 cm length and 20.0 cm height (figure 1(a)). Acrylic rods passing through holes in each slab align them. The phantom was placed on a 30.0 × 30.0 × 10.0 cm^3 solid water block (SolidWater® HE, Gammex Inc., Sun Nuclear, Middleton, WI, USA) with the longest axis of the phantom aligned parallel to B_0 (figure 1(b)). The solid water elevated the phantom so that its midplane was at the MRL isocentre, 14.0 cm above the couch. Using the on-board mega-voltage imager (MVI), A–P and L-R images were used to position the phantom apex 3.2 cm superior to the isocentre.

To measure ESE dose, EBT3 film strips (Ashland ISP Advanced Materials, NJ, USA) 25.0 × 7.5 cm^2 were positioned on a 30.0 × 30.0 × 5.0 cm^3 solid water slab, 5.0 cm superior to the phantom apex (figure 1(b)). Films were aligned with the long axis horizontal and with the midpoint approximately 14.0 cm above the couch. Markers were drawn on the film to indicate the position relative to the X and Z axes. A 30.0 × 30.0 × 0.1 cm^3 sheet of solid water and a dummy film (thickness 0.27 mm) were placed over each film strip (film effective depth of measurement 0.13 mm) to achieve a measurement depth of 1.4 mm (figure 2(a)), comparable to the depth of Monaco dose simulations (see below). With the gantry at 90.0° (G90) OFD generated by 1.0 × 1.0 cm^2, 2.0 × 2.0 cm^2, 3.0 × 3.0 cm^2, 4.0 × 4.0 cm^2 and 5.0 × 5.0 cm^2 beams, 1000 MU, was captured on film. As the

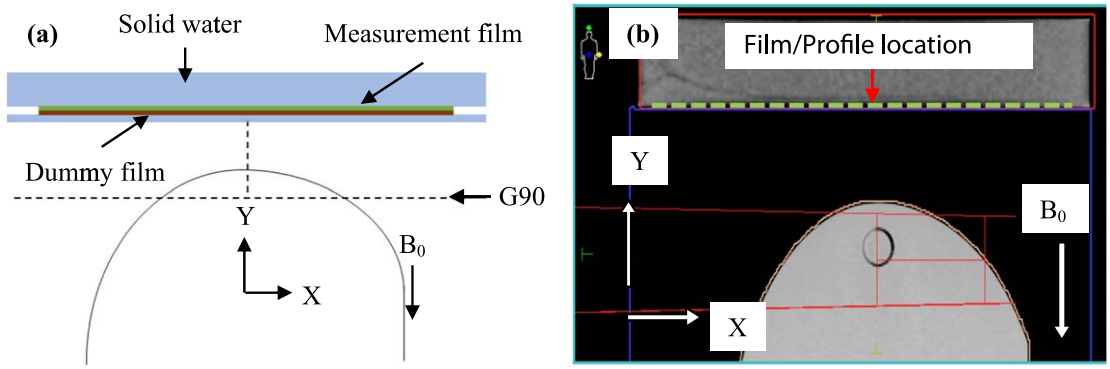

Figure 2. (a) Experimental schematic used to generate OFD (coronal view, not to scale) and (b) the simulation geometry with the 5.0 × 5.0 cm^2 field from G90 shown in red. For both, the positive Z axis is directed out of the page.

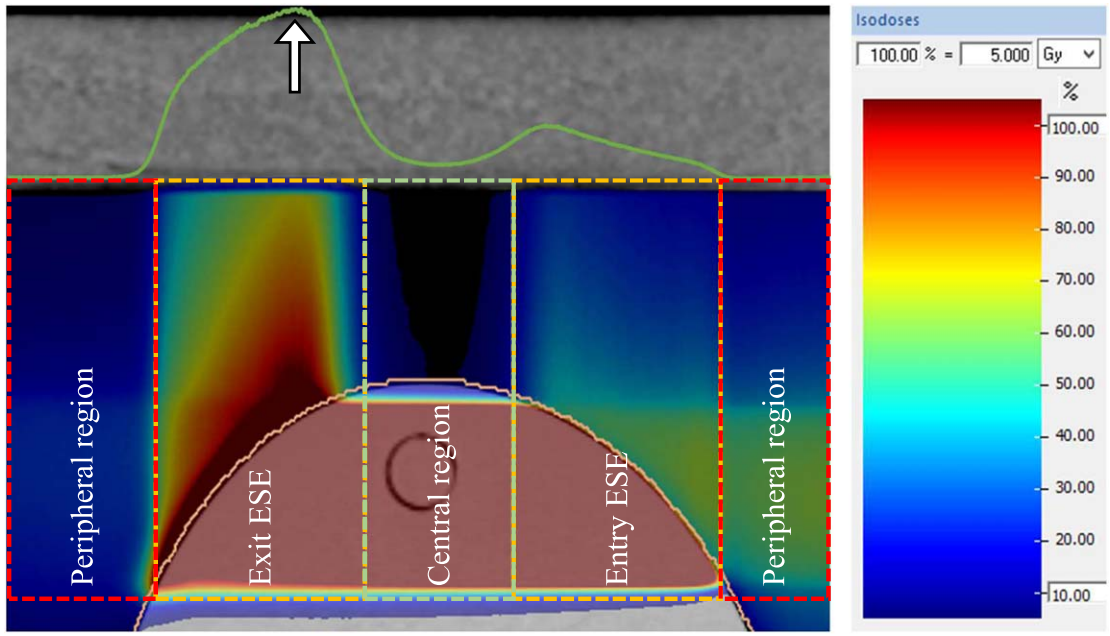

Figure 3. TPS visualization (coronal view) of OFD for a 5.0 × 5.0 cm^2 beam, G90 and the corresponding film profile with the different regions highlighted. The arrow indicates the location at which the vertical profile was extracted for this field size.

phantom curvature is asymmetric at the beam entrance and exit, OFD for a 5.0 × 5.0 cm^2 beam from G270 was additionally measured.

Film calibration was performed using 4.0 × 2.0 cm^2 strips and exposures 0, 50, 100, 200 and 400 MU, at 5.0 cm depth in solid water, 138.5 cm source-to-surface distance (SSD). Films were scanned using an Epson 12000XL Expression (Epson, Seiko Corporation, Japan) and images analysed using FilmQA^{TM} Pro software (Ashland ISP Advanced Materials, NJ, USA) and triple channel analysis (Lewis *et al* 2012). Off-axis response variation of the scanner was corrected (Lewis and Chan 2015). For each calibration film, a central region of interest (ROI) of approximately 1.0 × 1.0 cm^2 was used to obtain a mean pixel value. Horizontal dose profiles of 3.0 mm width were acquired through the centre of the OFD films, parallel to the long axis of each strip. Doses were normalized to the nominal D_{max} dose to water for a 5.0 × 5.0 cm^2 field, 1000 MU, SSD of 133.5 cm. In addition, profiles perpendicular to the beam direction (vertical), through OFD associated with the beam exit, were also determined for each G90 beam. The lateral location of the profiles was taken through the horizontal profile peak dose (see figure 3). These were normalized to the maximum dose along the profile.

Monaco simulations

The Monaco v5.40 treatment planning system, used in conjunction with the Unity, utilises a GPU based Monte Carlo dose algorithm (GPUMCD) providing rapid dose calculations in the presence of a static 1.5 T magnetic

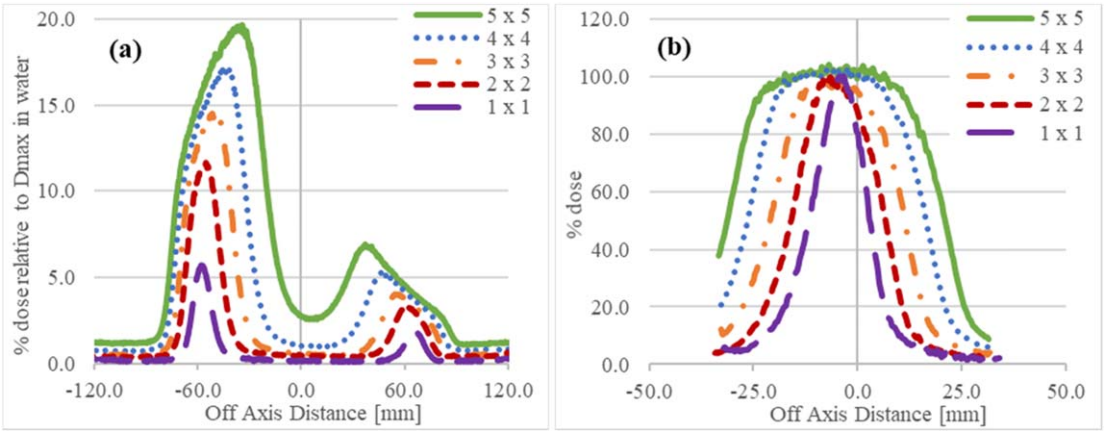

Figure 4. Measured film profiles for the various fields investigated. (a) shows the horizontal profiles, normalized to the nominal D_{max} dose to water for a 5.0 × 5.0 cm^2 field. In (b) the vertical profiles are shown, with the 5.0 × 5.0 cm^2 and 4.0 × 4.0 cm^2 normalized to central readings and smaller fields to the maximum recorded value.

field (Hissoiny *et al* 2011, Ahmad *et al* 2016). Dose calculations are performed on voxelized representations of patient, or phantom, CT/MR datasets. For CT based planning relative electron density (RED) is usually assigned to each voxel based on the CT number to RED conversion (i.e. 'unforced'); however, optional user assignment of RED to structures (i.e. 'forced') is available. REDs for structures are typically forced in MR planning, possibly using the mean RED derived from a CT scan. In both cases, REDs are converted to mass densities with the result mapped to chemical composition using Patient, Phantom or Couch material look-up tables. Users control calculation accuracy by specifying dose grid resolution and statistical uncertainty.

A CT dataset (1.0 mm slice thickness) of the experimental setup was imported to the TPS. The curved phantom was set as the external contour and the RED was unforced. The solid water slab used for film measurements, and the air between this structure and the phantom, were contoured. The former was assigned a forced RED of 1.000. Simulations were performed with either (a) the air structure RED unforced so values would approach 0.001, or (b) the air forced to 0.010. These were selected since with MR based planning an RED of 0.010 is the minimum value that can be assigned/forced, whilst for CT based planning the minimum is set by the CT to RED conversion.

The TPS isocentre was set to match the experimental setup. Figure 2(b) shows a screenshot of the TPS simulation set up for the 5.0 × 5.0 cm^2, G90 beam. Simulations for all beams were performed using a 0.1 cm dose grid, 0.2% per control point statistical uncertainty and the phantom look-up table. Due to set up uncertainties it was estimated that a ±1.0 mm offset (*Y* direction) could exist between the simulation and experimental phantom positions. Consequently, simulations for all fields were repeated with these shifts in the TPS isocentre. Due to the grid resolution transverse dose scoring planes at depth 1.5 mm in the solid water slab (approximating to the 1.4 mm measurement depth) were extracted for all TPS simulations. Verisoft v7.2 (PTW, Freiburg, Germany) was used to extract profiles from each dose plane and normalized as for film. Horizontal and vertical profiles were obtained for each field, at the same locations as described above for film measurements. Simulated profiles were compared to corresponding film profiles and difference plots (simulated—measured) were generated.

Results

Phantom OFD measurements

Figure 3 shows the dose distribution within and around the phantom for a 5.0 × 5.0 cm^2 beam, G90. The corresponding OFD horizontal film profile is shown. For all G90 beams, horizontal and vertical film profiles are shown in figure 4. Horizontal profiles (figure 4(a)) are centred about the isocentric *Y*–*Z* plane and extend in ±*X* directions. Peak doses are evident at the beam entrance and exit from the phantom. For each field, OFD peak dose is largest at the beam exit and a field size dependence of OFD is evident. As the field size is decreased, the width of the peak dose regions decreases and peak doses (entry and exit) for the G90 beam are greater than the corresponding G270 doses. The maximum observed OFD dose was approximately 20.0% of the D_{max} dose (figures 4 and 5). In the central region, measured dose for the G90 5.0 × 5.0 cm^2 field is approximately 2.6% of the D_{max} dose to water, significantly larger than for smaller fields (figure 4(a)). In peripheral regions (beyond

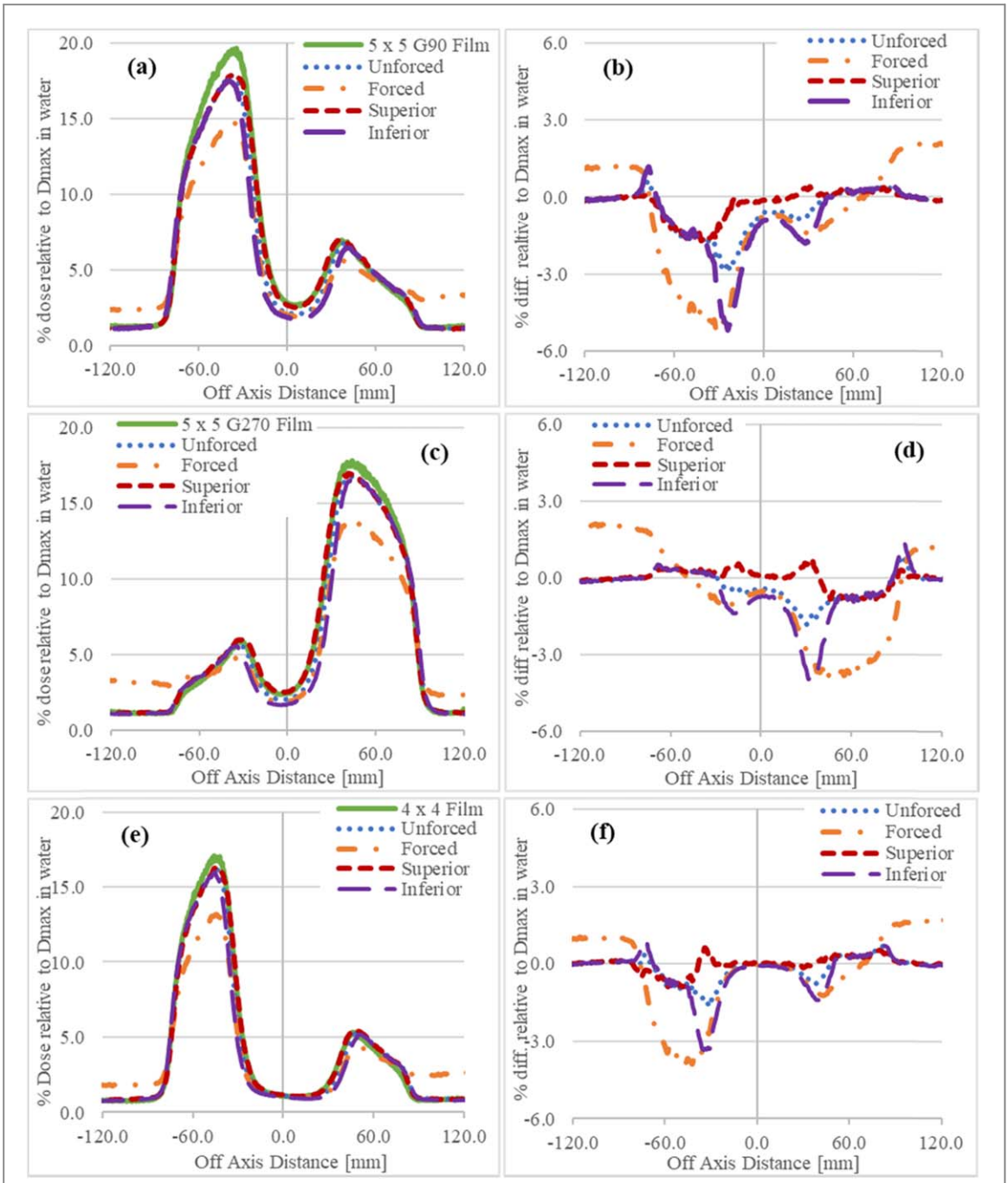

Figure 5. Calculated and measured horizontal profiles for (a) G90 5.0 × 5.0 cm^2 data, and (b) associated differences to film, with (c) showing the G270 5.0 × 5.0 cm^2 and (d) differences. Similarly, (e) shows the 4.0 × 4.0 cm^2 data and (f) differences. Values are expressed as a percentage of the nominal D_{max} dose to water for a 5.0 × 5.0 cm^2 field.

±90.0 mm), dose for the 5.0 × 5.0 cm^2 is approximately 1.3% of the D_{max} dose to water, again greater than the corresponding dose for smaller fields.

Vertical profiles through the horizontal peak dose at the exit of each G90 beam are shown in figure 4(b), centred about the isocentric X–Y plane and extending in ±Z directions. For the 5.0 × 5.0 cm^2 and 4.0 × 4.0 cm^2 fields, film noise was more apparent, and interfered with normalizing to the maximum dose in the profile; hence, the dose from $Z = 0.0$ mm was used instead. The peak of each profile is offset from the midplane of the phantom ($Z = 0.0$ mm), with offsets being more pronounced for smaller fields (3.0 × 3.0 cm^2 and below).

TPS and measured profile comparison

Figures 5 and 6 show comparisons of measured and simulated horizontal profiles. Figure 5(a) shows measured and simulated OFD profiles for the 5.0 × 5.0 cm^2 field, G90, and differences (simulated—measured) are presented in figure 5(b). With air RED unforced, differences are reduced relative to forced RED in peak dose

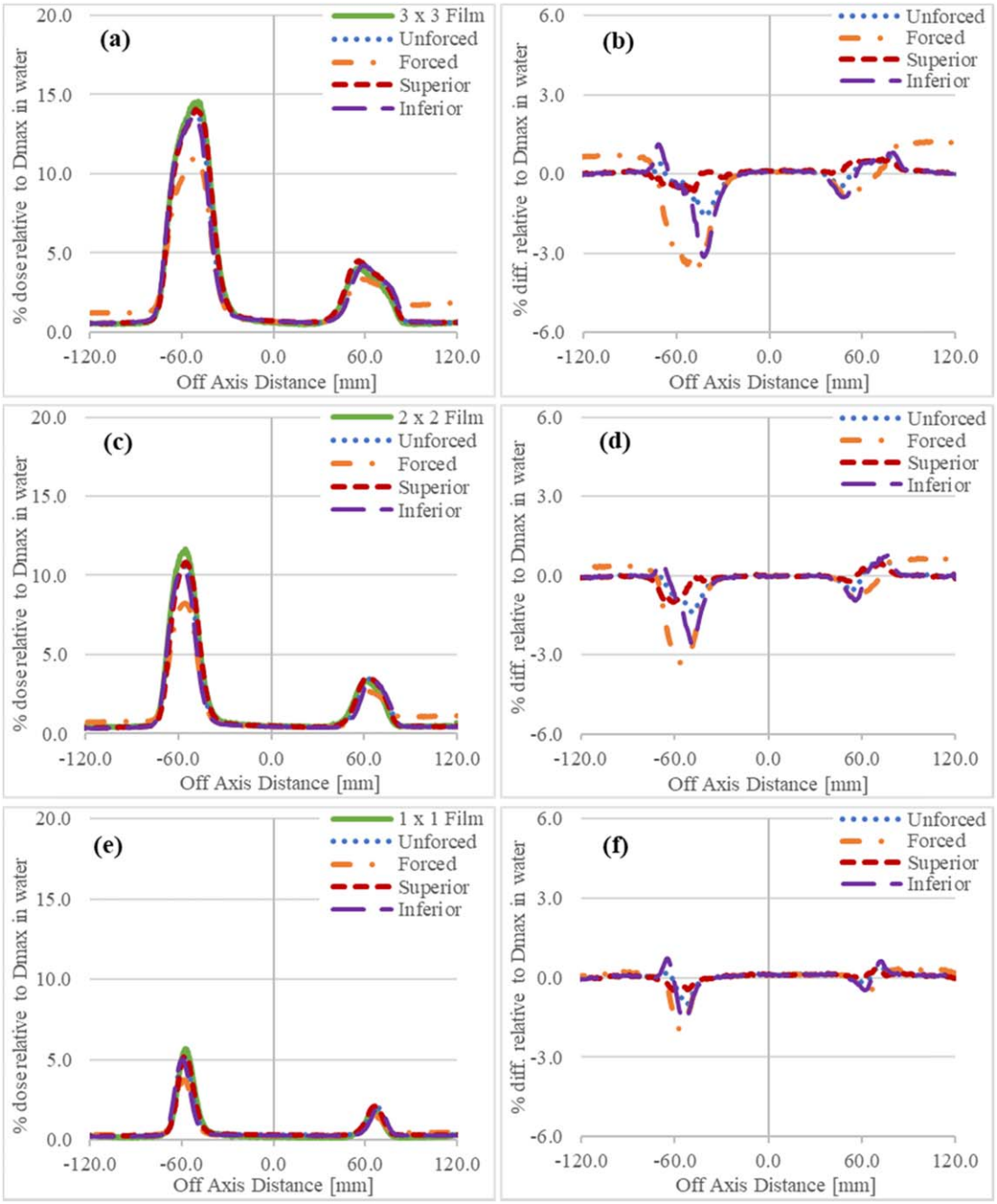

Figure 6. Calculated and measured doses for the phantom ESE with the (a) the 3.0 × 3.0 cm^2 field and (b) differences of calculations to film. Similarly, for the (c) 2.0 × 2.0 cm^2 and (d) differences, and (e) 1.0 × 1.0 cm^2 and (f) differences. Values are expressed as a percentage of the nominal D_{max} dose to water for a 5.0 × 5.0 cm^2 field.

regions, and this was observed across all field sizes and the G270 beam (figures 5 and 6). Beyond ±90.0 mm forced RED profile differences are greater than corresponding unforced simulations. OFD in these regions is overestimated with forced RED and this discrepancy is reduced with decreasing field size.

With unforced RED and the 1.0 mm superior shift, differences between the TPS and measured profiles are within the range −1.7% to 0.7% of D_{max} in water. The greatest difference is observed for the G90 5.0 × 5.0 cm^2 field. Excluding this field, differences are within −1.0% to 0.7% of D_{max} in water. Without the isocentre shift, differences were between −2.9% to 0.9% of D_{max}, and were even greater for the 1.0 mm inferior shift, at −5.2% to 1.4% of D_{max}. For the 5.0 × 5.0 cm^2 beam, measured entrance electron streaming dose is greater at G90 compared to G270 and this is consistent with corresponding TPS simulations.

In profile peripheries, differences for unforced RED simulations are independent of ±1.0 mm shifts and are within the range −0.16% to 0.10% of D_{max} in water. Difference plots in figure 6 show that in the central regions (up to ±40.0 mm for the 1.0 × 1.0 cm^2 field) profile differences approach 0.0%, independent of the Y-shift.

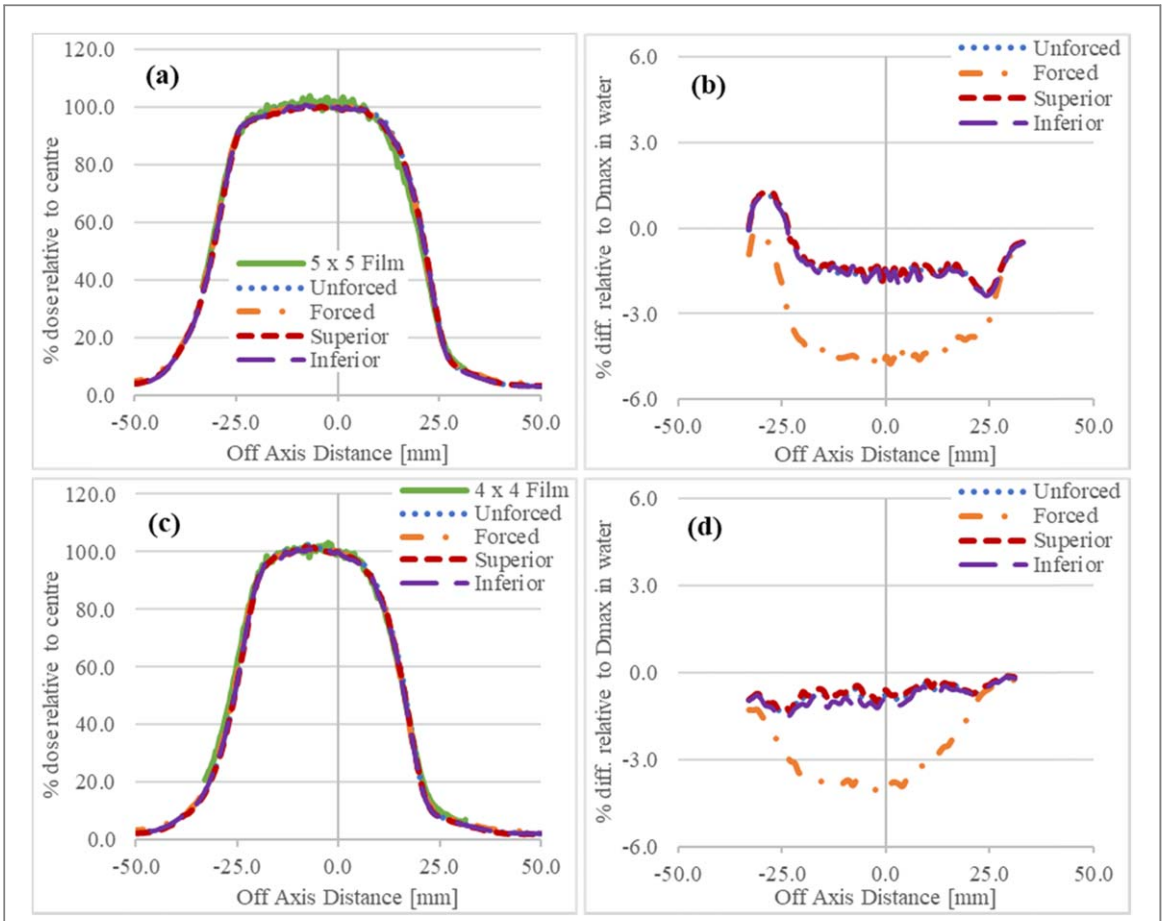

Figure 7. Calculated and measured vertical profiles for the (a) 5.0 × 5.0 cm^2 field with (b) associated differences to film, and (c) the 4.0 × 4.0 cm^2 field and (d) differences. Profiles in (a) and (c) have been normalized to the central value, and percentage differences in (c) and (d) are relative to the D_{max} dose to water for a 5.0 × 5.0 cm^2 field.

Vertical profiles for film and TPS simulations are shown in figures 7 and 8 for both REDs. Forced RED profile differences (simulated—measured) are greater than with unforced RED for all field sizes; however, differences with isocentre shifts showed minimal change. The greatest differences compared to film, with forced RED, were observed for the 5.0 × 5.0 cm^2 field.

Discussion

In general, the OFD horizontal profiles for all field sizes investigated exhibit the same features. Thus, for the purpose of discussion consider the G90 5.0 × 5.0 cm^2 measured dose profile. For this field the OFD profile as measured with film is shown in figure 5. Contributions to dose on the film can be attributed to head leakage and scatter (all regions), as well as SCE and ESE (in specific regions). Prior to beam incidence on the phantom the beam generates electrons in the air. These electrons give rise to SCE and contribute to dose deposition in the peripheral regions beyond ±90.0 mm. As the beam enters the phantom secondary electrons are produced with an estimated mean energy of 500.0 keV (Raaijmakers *et al* 2005) and an average range of 1.5 mm in acrylic (Berger *et al* 2017). Thus, it is reasonable to suggest that backscattered secondary electrons within this depth from the surface may escape into air. Dose due to ESE, and SCE generated by the beam before entry, is deposited in the region of approximately 20.0 mm to 100.0 mm. In the central region (approximately ±20.0 mm for the 5.0 × 5.0 cm^2 field) the beam edge is nominally 0.7 mm from the phantom apex. Due to the phantom curvature in this region, secondary electrons increasingly escape from the phantom on either side of the apex. This is evident from the in-air dose distribution in the region of the apex (figure 3). At the beam exit, forward scattered electrons at and near the surface appear to enter air. As a result, ESE dose deposition occurs in the region of −20.0 to −90.0 mm. SCE may in part contribute to OFD in this region. As the field size decreases, in-air and in-phantom Compton interactions decrease; hence, the magnitude of SCE and ESE decreases. As a result of Compton interactions within the phantom, forward and backscattered electrons contribute to ESE at the beam exit and entrance, respectively. Albeit that the beam is attenuated within the phantom, the larger exit ESE dose

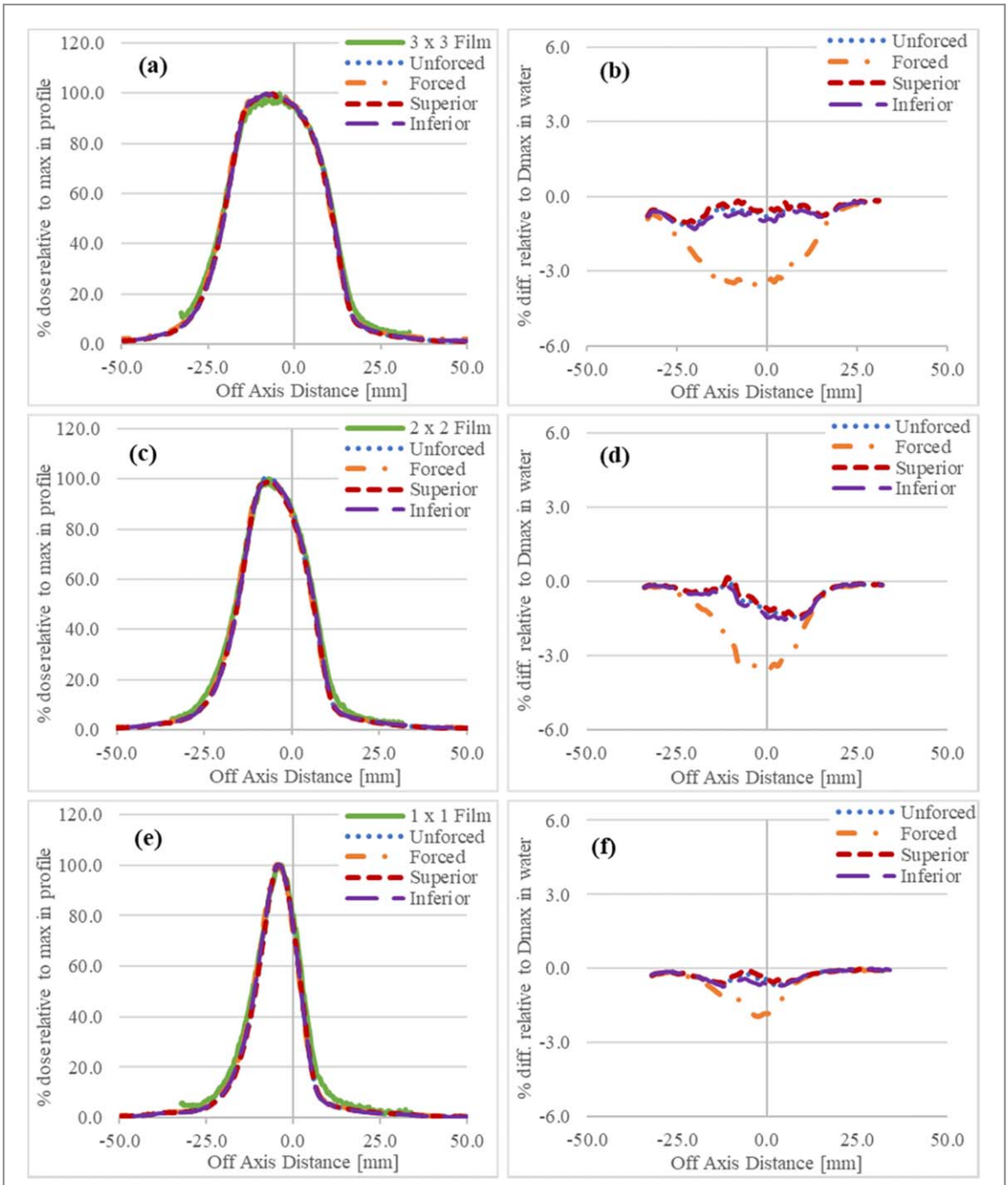

Figure 8. Calculated and measured vertical profiles for the (a) 3.0 × 3.0 cm^2 field with (b) associated differences to film, (c) the 2.0 × 2.0 cm^2 field and (d) differences and (e) 1.0 × 1.0 cm^2 field, with (f) differences. Values in (a), (c) and (e) have been normalized to the maximum value in the profile, and percentages in (b), (d) and (f) are relative to the D_{max} dose to water for a 5.0 × 5.0 cm^2 field.

observed for all field sizes suggests the dominance of forward scattered electrons, consistent with previous investigations (Malkov *et al* 2019b, Powers 2022).

With a forced RED (0.010) differences between simulated and measured ESE doses are greater than with unforced RED (0.001). This is particularly evident for exit ESE and is consistent with increased in-air attenuation of streaming electrons in forced RED simulations. At profile peripheries, the simulated SCE contribution to OFD is overestimated with forced RED. Forced RED simulations would tend to overestimate in-air Compton interactions and attenuation of streaming electrons. The enhancement of Compton-electron production appears to be the dominant process given that SCE is overestimated. Further investigation outside the scope of this work is needed to confirm this. Clinically for MR-based planning, internal air structures may be forced to the minimum RED of 0.010. Consequently, simulations of OFD will tend to underestimate ESE and overestimate SCE. However, such discrepancies do not inhibit the identification of patient shielding requirements.

Differences between simulated (unforced RED) and measured profiles for 5.0 × 5.0 cm^2 G90 and G270 beams are influenced by the ±1.0 mm isocentre shifts. Dose in the central region is sensitive to the proximity of

the field edge to the phantom apex. With a 1.0 mm superior shift, simulated and measured OFD discrepancies were decreased. Discrepancies for other field sizes are less sensitive to superior and inferior shifts. For these fields the separation of the curved surface from each field edge is greater than that of the largest field, discussed above. Isocentre shifts appear to affect ESE peaks significantly, with reduced differences observed with the introduction of the 1.0 mm superior shift. It is worth noting, even with consistent isocentre positioning, some variation in OFD would still be expected due to the difference between measurement and simulation depths. Differences between exit electron streaming dose for the G90 and G270 beams is associated with the larger radius of curvature of the phantom surface for the latter beam and is consistent with previous observations (Malkov *et al* 2019a). TPS simulations of exit dose for these beams exhibit similar differences.

Unforced RED vertical profile simulations are in good agreement with measured data, independent of the $\pm$1.0 mm shifts. Differences (simulated—measured) were less than 2.0% of the D_{max} dose to water, for the largest field, and typically decreased with field size. Larger differences were observed in the penumbral regions, where grid resolution and modelling uncertainties would tend to have the greatest impact. Forced RED vertical profile simulations showed increased differences relative to film, consistent with horizontal profiles. Relative to the central beam axis the midpoints of the profiles are shifted in the $-Z$ direction, the same direction as the Lorentz force in this experimental arrangement.

Conclusion

In this work OFD approximately 20% of the D_{max} dose to water was observed and was attributed to streaming electrons. For all fields investigated, TPS simulated and measured OFD discrepancies are in good agreement. Discrepancies between measurement and simulated data are influenced by experimental set up uncertainties. The influence of surface curvature on measured ESE has been demonstrated and is consistent with TPS simulations. The use of unforced RED for air in TPS simulations of SCE and ESE is recommended for improved accuracy.

Acknowledgments

The authors wish to acknowledge that parts of this work have been presented in Marcus Powers' PhD Thesis at James Cook University. No funding was obtained for the preparation of this manuscript. The authors have contributed equally and share first authorship.

Data availability statement

The data cannot be made publicly available upon publication because no suitable repository exists for hosting data in this field of study. The data that support the findings of this study are available upon reasonable request from the authors.

Ethical statement

This manuscript does not contain any studies performed on humans or animals.

ORCID iDs

Marcus Powers https://orcid.org/0000-0002-4235-6123
John Baines https://orcid.org/0000 0002 5013 1100

References

Ahmad S, Sarfehnia A, Paudel M, Kim A, Hissoiny S, Sahgal A and Keller B 2016 Evaluation of a commercial MRI Linac based monte carlo dose calculation algorithm with geant 4 *Med. Phys.* **43** 894–907

Baines J, Powers M and Newman G 2021 Sources of out-of-field dose in MRgRT: an inter-comparison of measured and Monaco treatment planning system doses for the Elekta Unity MR-linac *Phys. Eng. Sci. Med.* **44** 1049–59

Berger M, Coursey J, Zucker M and Chang J 2017 Stopping Power and Range Tables for Electrons, Protons and Helium Ions *National Institute of Standards and Technology (NIST)* Accessed March 2020

De-Colle C *et al* 2021 Analysis of electron-stream effect in patients with partial breast irradiation using a 1.5 T MR-linear accelerator *Clin. Transl. Radiat. Oncol.* **27** 103–8

Hackett S, van Asselen B, Wolthaus J, Bluemink J, Ishakoglu K, Kok J, Lagendijk J and Raaymakers B 2018 Spiraling contaminant electrons increase doses to surfaces outside the photon beam of an MRI-linac with a perpendicular magnetic field *Phys. Med. Biol.* **63** 095001

Hissoiny S, Raaijmakers A, Ozell B, Després P and Raaymakers B 2011 Fast dose calculation in magnetic fields with GPUMCD *Phys. Med. Biol.* **56** 5119
Lewis D, Micke A, Yu X and Chan M 2012 An efficient protocol for radiochromic film dosimetry combining calibration and measurement in a single scan *Med. Phys.* **39** 6339–50
Lewis D and Chan M 2015 Correcting lateral response artifacts from flatbed scanners for radiochromic film dosimetry *Med. Phys.* **42** 416–29
Lui H, Ding S, Wang B, Li Y, Sun Y and Huang X 2020 In-air electron streaming effect for esophageal cancer radiotherapy with a perpendicular magnetic field: a treatment planning study *Front.Oncol.* **10** 607061
Malkov V, Hackett S, Asselen B, Raaymakers B and Wolthaus J 2019a Monte Carlo simulations of out-of-field skin dose due to spiralling contaminant electrons in a perpendicular magnetic field *Med. Phys.* **46** 1467–77
Malkov V, Hackett S, Wolthaus J, Raaymakers B and van Asselen B 2019b Monte Carlo simulations of out-of-field surface doses due to the electron streaming effect in orthogonal magnetic fields *Phys. Med. Biol.* **64** 115029
Nachbar M *et al* 2020 Partial breast irradiation with the 1.5 T MR-Linac: first patient treatment and analysis of electron return and stream effects *Radiother. Oncol.* **145** 30–5
Park J, Shin K, Kim J, Park S, Jeon S, Choi N, Kim J and Wu H 2018 Air-electron stream interactions during magnetic resonance IGRT: skin irradiation outside the treatment field during accelerated partial breast irradiation *Strahlentherapie Onkol.* **194** 50–9
Powers M 2022 Commissioning and out-of-field dose characterisation of the elekta unity MRL *PhD thesis* James Cook University Townsville (https://doi.org/10.25903/0qbp-gr53)
Powers M and Baines J 2022 Electron streaming effect associated with the elekta unity anterior imaging coil *Front. Phys.* **10** 880121
Raaijmakers A, Raaymakers B and Lagendijk J 2005 Integrating a MRI scanner with a 6 MV radiotherapy accelerator: dose increase at tissue-air interfaces in a lateral magnetic field due to returning electrons *Phys. Med. Biol.* **50** 1363–76
Raaymakers B W *et al* 2009 Integrating a 1.5 T MRI scanner with a 6 MV accelerator: proof of concept *Phys. Med. Biol.* **54** N229
Raaymakers B W *et al* 2017 First patients treated with a 1.5 T MRI-Linac: clinical proof of concept of a high-precision, high-field MRI guided radiotherapy treatment *Phys. Med. Biol.* **62** L41–L50
Snyder J, St-Aubin J, Yaddanapudi S, Boczkowski A, Dunkerley D, Graves S and Hyer D 2020 Commissioning of a 1.5T elekta unity MR-linac: a single institution experience *J. Appl. Clin. Med. Phys.* **21** 160–72
Woodings S *et al* 2021 Acceptance procedure for the linear accelerator component of the 1.5 T MRI-linac *J. Appl. Clin. Med. Phys.* **22** 45–59